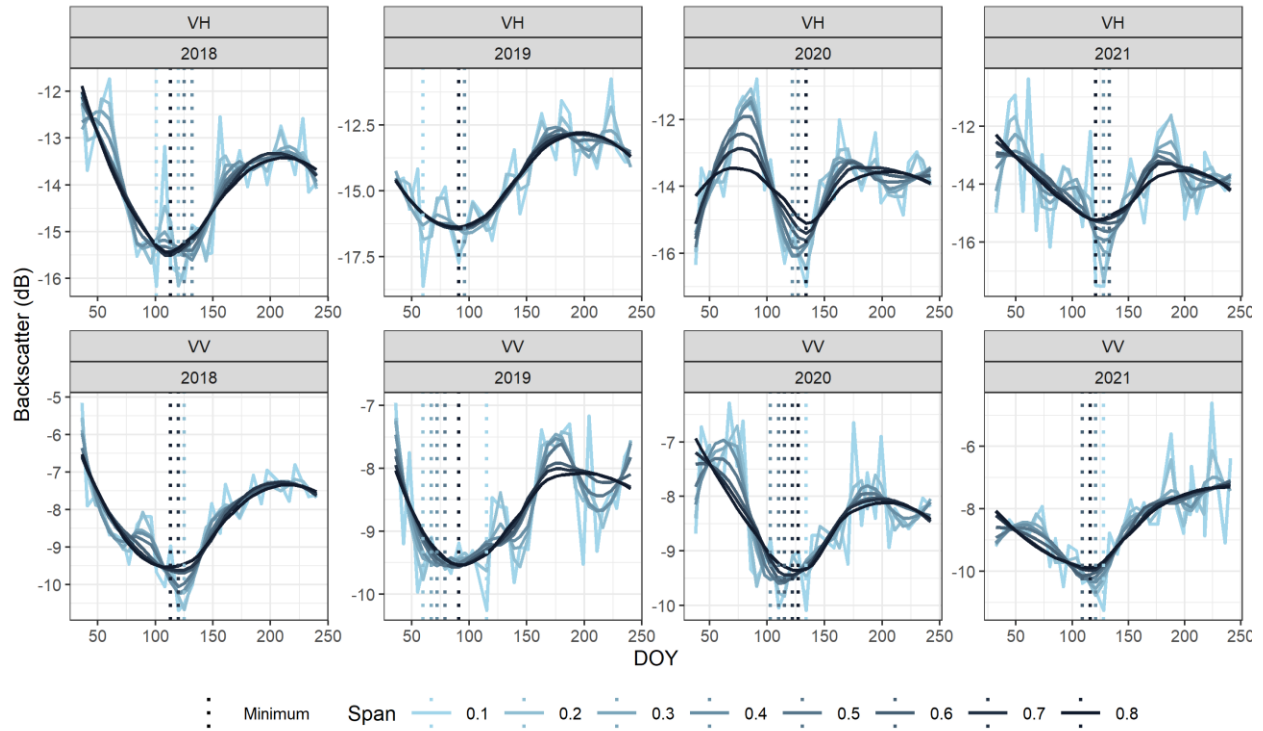
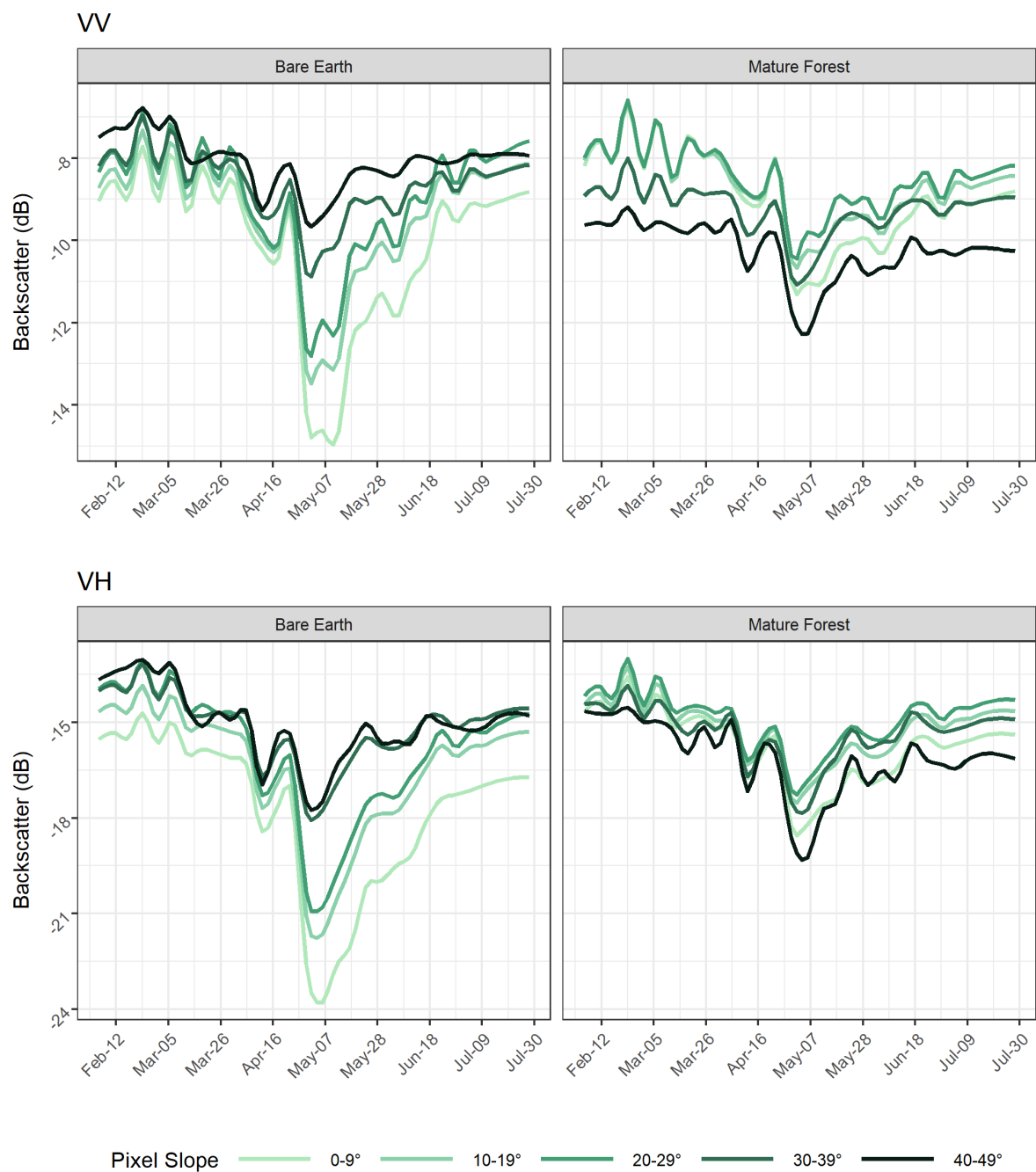


**Figure S1.** The impact of span on loess regressions of Sentinel-1 SAR signals at Downton Lake Upper. Minima in time series are denoted with dotted lines for VH polarized timeseries (top) and VV polarized timeseries (bottom). Larger spans push minima later into the summer and miss the initial sensitivity of SAR backscatter to melt onset or snowpack ripening. Spans of less than 0.2 should be avoided, however, as they are too sensitive to noise in SAR signals.



**Figure S2.** The impact of span on loess regressions of Sentinel-1 SAR signals at Green Mountain. Minima in time series are denoted with dotted lines for VH polarized timeseries (top) and VV polarized timeseries (bottom). Larger spans push minima later into the summer and miss the initial sensitivity of SAR backscatter to melt onset or snowpack ripening. Spans of less than 0.2 should be avoided, however, as they are too sensitive to noise in SAR signals.



**Figure S3.** SAR backscatter time series in the Lajoie Basin from pixels located between 1600 and 1800 m from VV (top) and VH (bottom) polarized images. Observations under mature forest cover are displayed on the right, whereas observations in open areas are displayed on the left. Average backscatter for each cover type is shown by the shaded lines, with each line representing a different slope category. Observations are from 2018.



**Figure S4.** SAR backscatter time series in the Lajoie Basin from pixels located between 1600 and 1800 m from VV (top) and VH (bottom) polarized images. Observations under mature forest cover are displayed on the right, whereas observations in open areas are displayed on the left. Average backscatter for each cover type is shown by the shaded lines, with each line representing a different slope category. Observations are from 2019.

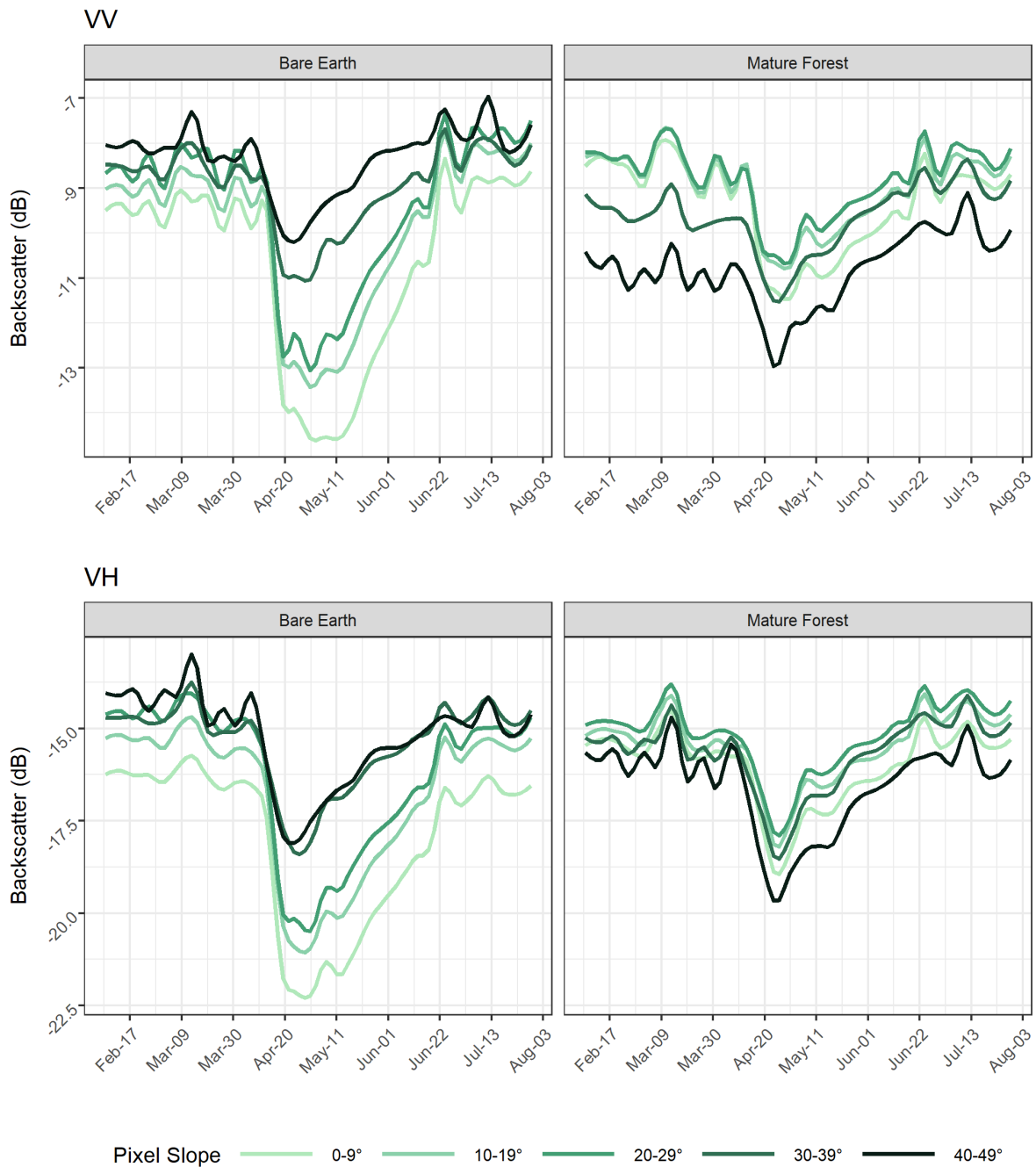


**Figure S5.** SAR backscatter time series in the Lajoie Basin from pixels located between 1600 and 1800 m from VV (top) and VH (bottom) polarized images. Observations under mature forest cover are displayed on the right, whereas observations in open areas are displayed on the left. Average backscatter for each cover type is shown by the shaded lines, with each line representing a different slope category. Observations are from 2020.

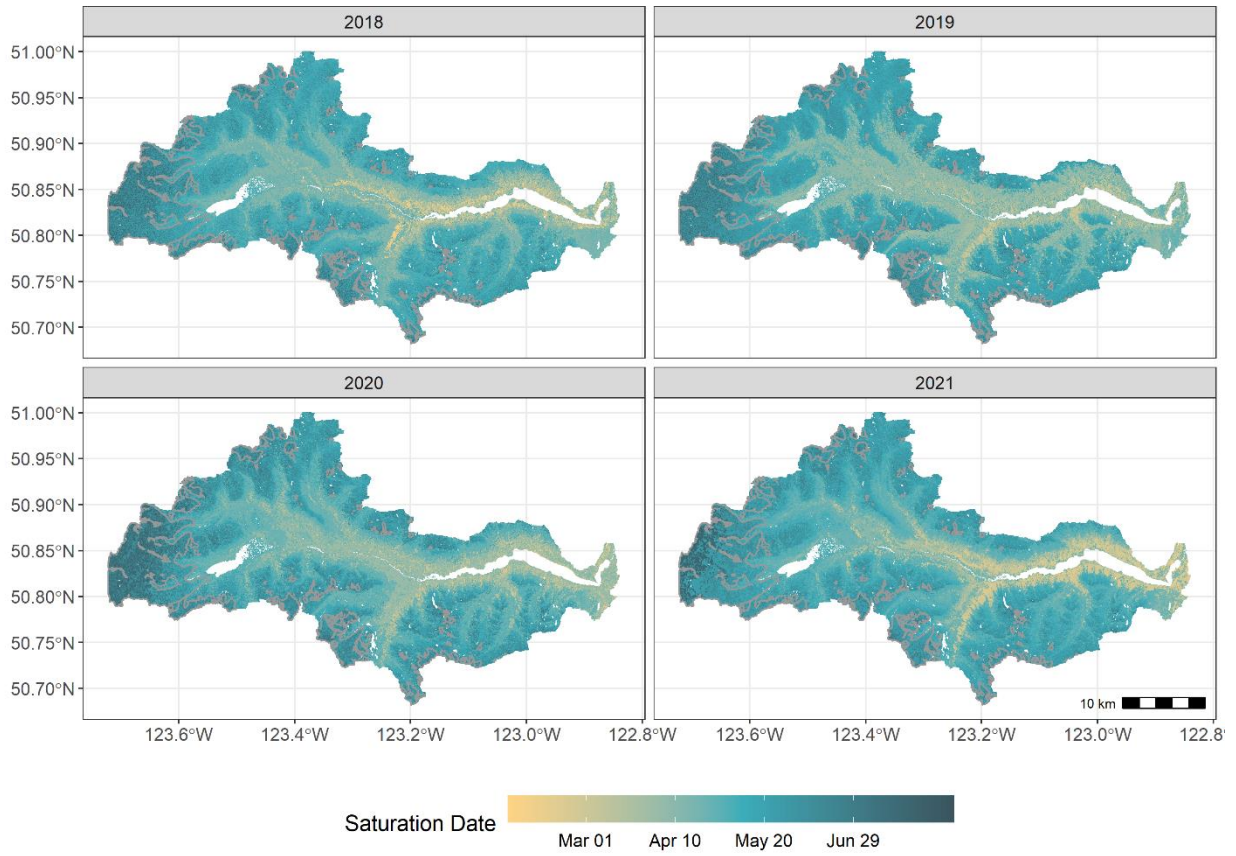


**Figure S6.** Estimates of snowpack saturation (snowmelt onset) from Sentinel-1 SAR in the Lajoie Basin. Snowmelt onset estimates are inferred from minima in SAR timeseries. Estimates are derived from VH polarized images.

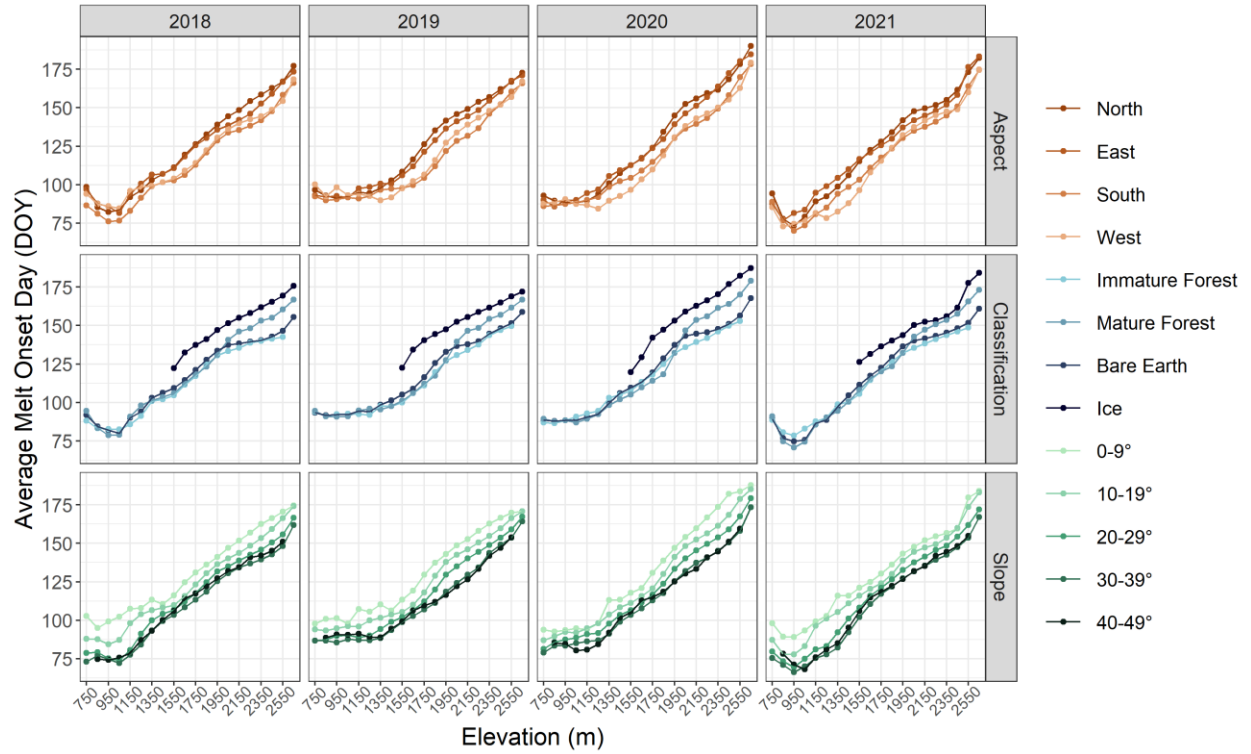


**Figure S7.** Average estimates of snowmelt onset by elevation, aspect, classification, and slope. Estimates of melt onset are inferred from minima in Sentinel-1 SAR time series. Estimates are derived from VH polarized images.

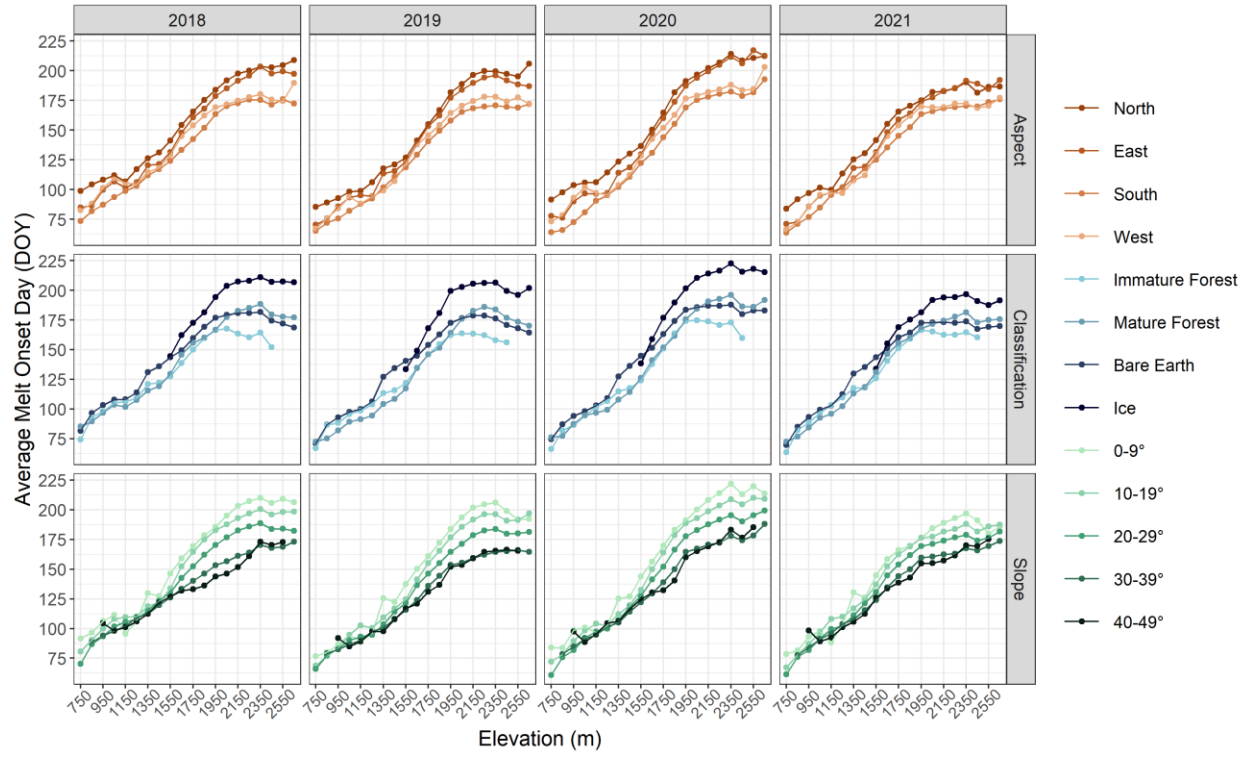


**Figure S8.** Average estimates of snow disappearance by elevation, aspect, classification, and slope. Estimates of melt onset are inferred from Landsat-8 and Sentinel-2 imagery.

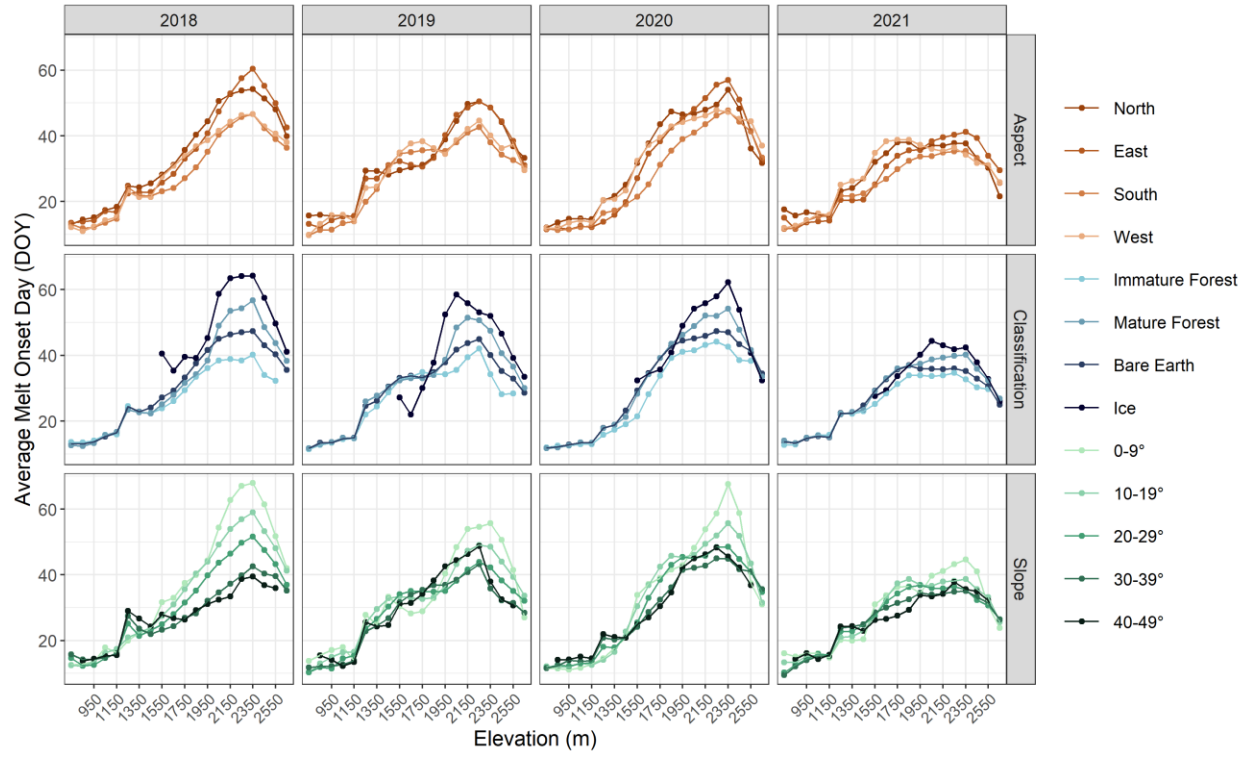


**Figure S9.** Average estimates of snowmelt duration by elevation, aspect, classification, and slope. Estimates of melt duration are from a fusion of SAR based estimates of melt onset and optical estimates of melt end. Averages are derived from VV polarized SAR images.

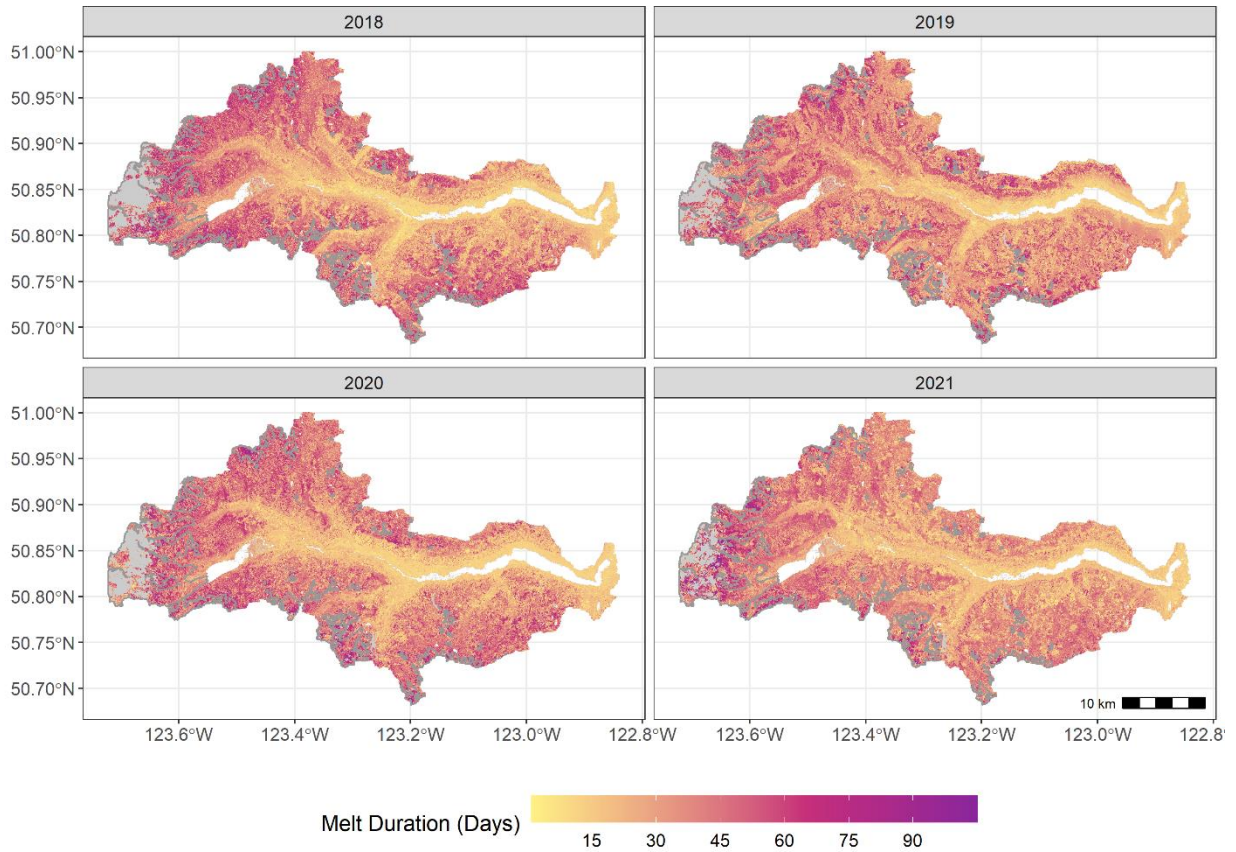


**Figure S10.** Snowmelt runoff duration in the Lajoie Basin from data fusion melt products. Durations are approximated by differencing radar estimates of snowmelt onset and optical/multispectral estimates of snow free dates. Gray shading represents perennial snow, and the grey outlines delineate glacierized areas. Estimates are derived from VH polarized SAR images.

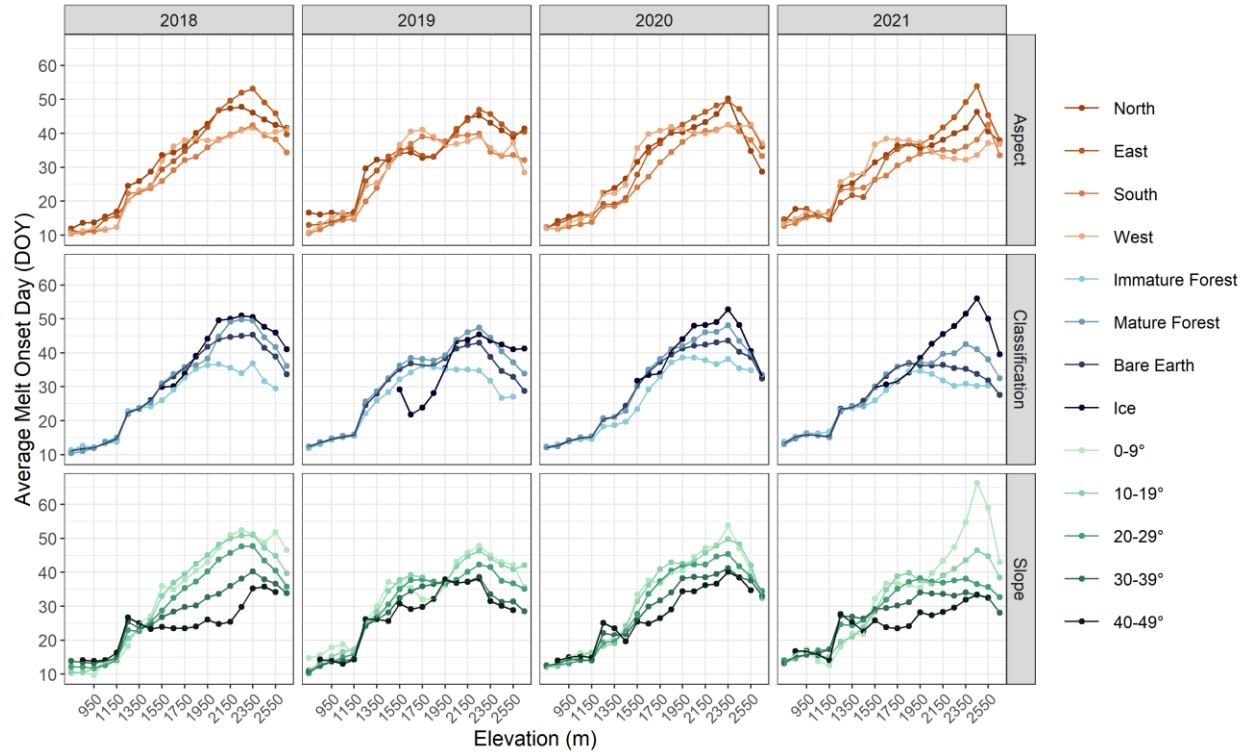


**Figure S11.** Average estimates of snowmelt duration by elevation, aspect, classification, and slope. Estimates of melt duration are from a fusion of SAR based estimates of melt onset and optical estimates of melt end. Averages are derived from VH polarized SAR images.

**Table S1.** Total corrected area for SAR estimates of melt onset, optical estimates of snow disappearance, and fusion estimates of melt duration.

	2018	2019	2020	2021
<b>Onset (km<sup>2</sup>)</b>	60.3	58.3	63.4	64.7
<b>Onset (%)</b>	6.2	5.6	6.5	6.6
<b>Melt End (km<sup>2</sup>)</b>	109.	116.6	121.6	134.8
<b>Melt End (%)</b>	11.1	11.9	12.4	13.8
<b>Duration (km<sup>2</sup>)</b>	191.8	257.9	204.1	230.9
<b>Duration (%)</b>	19.6	26.3	20.5	23.6

**Table S2.** Comparison of data fusion and SWE estimates of snowmelt end, onset and duration at Downton Lake Upper. The difference in days is provided between telemetry based (TLM) estimates of melt, and SAR, optical (OPT) and data fusion estimates of melt. SAR results are from VH polarized images.

	2018	2019	2020	2021
<b>Onset (TLM)</b>	May 5	May 8	May 4	May 10
<b>Onset (SAR)</b>	May 17	Apr 6	April 24	April 26
<b>Difference (Days)</b>	12	32	10	14
<b>Melt End (TLM)</b>	June 24	June 17	June 24	June 26
<b>Melt End (OPT)</b>	June 19	June 14	June 16	June 8
<b>Difference (days)</b>	5	3	8	18
<b>Duration (TLM)</b>	50	40	51	47
<b>Duration (Fusion)</b>	33	69	53	19
<b>Difference (days)</b>	17	29	2	28

**Table S3.** Comparison of data fusion and SWE estimates of snowmelt end, onset and duration at Green Mountain. The difference in days is provided between telemetry based (TLM) estimates of melt, and SAR, optical (OPT) and data fusion estimates of melt. SAR results are from VH polarized images.

	2018	2019	2020	2021
<b>Onset (TLM)</b>	April 29	April 30	May 7	May 13
<b>Onset (SAR)</b>	April 30	May 19	May 6	May 13
<b>Difference (Days)</b>	1	18	1	0
<b>Melt End (TLM)</b>	June 3	June 3	June 9	June 9
<b>Melt End (OPT)</b>	June 17	March 29	May 18	June 1
<b>Difference (days)</b>	14	66	22	7
<b>Duration (TLM)</b>	35	33	33	27
<b>Duration (Fusion)</b>	48	36	12	34
<b>Difference (days)</b>	13	3	21	7